

Cumulative physical uncertainty in modern stellar models (Research Note)

II. The dependence on the chemical composition

G. Valle¹, M. Dell’Omodarme¹, P.G. Prada Moroni^{1,2}, S. Degl’Innocenti^{1,2}

¹ Dipartimento di Fisica “Enrico Fermi”, Università di Pisa, largo Pontecorvo 3, Pisa I-56127 Italy

² INFN, Sezione di Pisa, Largo B. Pontecorvo 3, I-56127, Italy

Received 21/01/2013; accepted 08/04/2013

ABSTRACT

Aims. We extend our previous work on the effects of the uncertainties on the main input physics for the evolution of low-mass stars. We analyse the dependence of the cumulative physical uncertainty affecting stellar tracks on the chemical composition.

Methods. We calculated more than 6000 stellar tracks and isochrones, with metallicity ranging from $Z = 0.0001$ to $Z = 0.02$, by changing the following physical inputs within their current range of uncertainty: ${}^1\text{H}(p, \nu e^+){}^2\text{H}$, ${}^{14}\text{N}(p, \gamma){}^{15}\text{O}$ and triple- α reaction rates, radiative and conductive opacities, neutrino energy losses, and microscopic diffusion velocities. The analysis was performed using a latin hypercube sampling design. We examine in a statistical way – for different metallicities – the dependence on the variation of the physical inputs of the turn-off (TO) luminosity, the central hydrogen exhaustion time (t_{H}), the luminosity and the helium core mass at the red-giant branch (RGB) tip, and the zero age horizontal branch (ZAHB) luminosity in the RR Lyrae region.

Results. For the stellar tracks, an increase in the metallicity from $Z = 0.0001$ to $Z = 0.02$ produces a cumulative physical uncertainty error variation in TO luminosity from 0.028 dex to 0.017 dex, while the global uncertainty on t_{H} increases from 0.42 Gyr to 1.08 Gyr. For the RGB tip, the cumulative uncertainty on the luminosity is almost constant at 0.03 dex, whereas the one the helium core mass decreases from $0.0055 M_{\odot}$ to $0.0035 M_{\odot}$. The dependence of the ZAHB luminosity error is not monotonic with Z , and it varies from a minimum of 0.036 dex at $Z = 0.0005$ to a maximum of 0.047 dex at $Z = 0.0001$. Regarding stellar isochrones of 12 Gyr, the cumulative physical uncertainty on the predicted TO luminosity and mass increases respectively from 0.012 dex to 0.014 dex and from $0.0136 M_{\odot}$ to $0.0186 M_{\odot}$. Consequently, from $Z = 0.0001$ to $Z = 0.02$ for ages typical of galactic globular clusters, the uncertainty on the age inferred from the TO luminosity increases from 325 Myr to 415 Myr.

Key words. methods: statistical – stars: evolution – stars: horizontal-branch – stars: interiors – stars: low-mass – stars: Hertzsprung-Russell and C-M diagrams

1. Introduction

The present paper extends the analysis presented in Valle et al. (2013) (hereafter PI) on the impact of the physical uncertainties affecting stellar evolution models to a wide range of chemical compositions covering the typical values for stellar populations in the Milky Way and in the near galaxies. As in the previous work, this paper is focused on the evolutionary characteristics of ancient stellar populations, and thus the analysis is restricted to stellar models of low-mass stars from the main sequence (MS) to the zero age horizontal branch (ZAHB).

In PI we determined, for a fixed chemical composition (metallicity $Z = 0.006$, and helium abundance $Y = 0.26$), the range of variation in some important evolutionary features due to the changes in the input physics within their uncertainty, pointing out the effect of the different physical inputs at different stages of stellar evolution.

The aim of this paper is to analyse how the results found in PI depend on the assumed chemical composition. Thus, we computed models covering a wide metallicity range, i.e. from $Z = 0.0001$ to 0.02 . We focus on the turn-off luminosity L_{BTO} , the central hydrogen exhaustion time t_{H} , the luminosity L_{tip} and the

helium-core mass M_{c}^{He} at the red giant branch (RGB) tip, and the ZAHB luminosity L_{HB} in the RR Lyrae region at $\log T_{\text{eff}} = 3.83$. As turn-off luminosity we adopted the luminosity of a point brighter and 100 K lower than the turn-off (hereafter BTO), a technique similar to the one proposed by Chaboyer et al. (1996) for isochrones in the (B-V, V) plane and already adopted in PI.

Table 1 lists the physical input that was allowed to vary and the assumed uncertainty on each. We refer to PI for a detailed discussion underlying their choice and the determination of the uncertainty ranges.

2. Description of the technique

We adopt a reference model of $M = 0.90 M_{\odot}$ to explore the cumulative effect of the uncertainty on the main input physics, for six different metallicity values, i.e. $Z = 0.0001, 0.0005, 0.001, 0.006, 0.01, \text{ and } 0.02$.

Determination of the initial helium abundances was done using a linear helium-to-metal enrichment law: $Y = Y_p + \frac{\Delta Y}{\Delta Z} Z$, with cosmological ${}^4\text{He}$ abundance $Y_p = 0.2485$ (Cyburt et al. 2004; Steigman 2006; Peimbert et al. 2007a,b). We adopted $\Delta Y/\Delta Z = 2$, as the typical value for this quantity, which is still affected by several important sources of uncertainty (Pagel & Portinari 1998; Jimenez et al. 2003; Flynn 2004; Gennaro et al. 2010).

Send offprint requests to: G. Valle, valle@df.unipi.it

Table 1. Physical inputs perturbed in the calculations and their assumed uncertainty. The abbreviations used in the following tables are defined in parentheses.

description	parameter	uncertainty
${}^1\text{H}(p,ve^+){}^2\text{H}$ reaction rate (pp)	p_1	3%
${}^{14}\text{N}(p,\gamma){}^{15}\text{O}$ reaction rate (${}^{14}\text{N}$)	p_2	10%
radiative opacity (k_r)	p_3	5%
microscopic diffusion velocities (v_d)	p_4	15%
triple- α reaction rate (3α)	p_5	20%
neutrino emission rate (ν)	p_6	4%
conductive opacity (k_c)	p_7	5%

Notes. The table is taken from PI and is reported for the reader’s convenience.

Thus, we computed models by adopting the following couples of initial metallicity and helium abundance (Z, Y): (0.0001, 0.249), (0.0005, 0.25), (0.001, 0.25), (0.006, 0.26), (0.01, 0.268), and (0.02, 0.288).

The adopted stellar evolutionary code, FRANEC, is the same as used in PI and for the construction of the Pisa Stellar Evolution Data Base¹ for low-mass stars (Dell’Omodarme et al. 2012). We refer to these papers and to Valle et al. (2009) for a detailed description of the input on the stellar evolutionary code and of the ZAHB construction technique.

We briefly recall the technique followed in PI, i.e. a systematic variation in the input physics on a fixed grid within their current uncertainty. For every physical input listed in Table 1, we adopted a three-value multiplier p_i with value 1.00 for the unperturbed case and values $1.00 \pm \Delta p_i$ for perturbed cases (Δp_i is the uncertainty listed in Table 1). For each stellar track calculation, a set of multiplier values (i.e. p_1, \dots, p_7) is fixed. Then, to cover the whole parameter space and explore all the possible interactions among input physics, calculations of stellar tracks must be performed for a full crossing, i.e. each parameter value p_i crossed with all the values of the other parameters p_j , with $j \neq i$.

However, as shown in PI, the interactions among the physical inputs are negligible for such small perturbations. This makes possible to reduce the computational burden by avoiding computation of the whole set of $3^7 = 2187$ tracks with the same mass, chemical composition, and α_{ml} for each metallicity. We select randomly – for each Z – a subset of $n = 162$ models to be computed using a latin hypercube sampling design: it is an extension of the latin square to higher dimensions and it has optimal property in reducing the variance of the estimators obtained from the linear models (Stein 1987). The sample size was chosen to balance the expected run time with good precision in the estimation of the effects of the input physics. In particular, we evaluated the impact of a sample size reduction on the significance of the estimated coefficients reported in PI. For this purpose, we considered that the estimated errors of the effects (see Sect. 3) of the input physics – hence the confidence intervals width of the effects – scale approximately as the square root of the ratio of the original sample size (i.e. 2187) and the subsample size n .

Test simulations, performed by extracting different samples of different size n and analysing the influence of the input physics in each sample, showed that the sample size $n = 162$ is sufficient to obtain robust estimates of the input physics impacts. The random selection was performed using the R library lhs (Carnell 2012), resulting in a total sample of 972 stellar tracks.

¹ <http://astro.df.unipi.it/stellar-models/>

3. Statistical analysis of physical uncertainty

Relying on such a large set of perturbed stellar models, we statistically analysed the effects of varying the physical inputs listed in Table 1 on the selected evolutionary features. For each Z value, we built linear regression models by extracting the values of the dependent variable under study (i.e. L_{BTO} , t_{H} , L_{tip} , M_{c}^{He} , and L_{HB}) from the stellar tracks and regressing them against the covariates, i.e. the values of the parameter p_i . Thus we stratified the sample according to Z values and we treated strata separately.

An alternative approach would require a global fit of the data, modelling the dependence on Z and Y by inserting of interaction terms into the statistical model; however, direct computations showed that the models of these dependencies are quite cumbersome and require a function with several powers of log-metallicity. We therefore prefer not to rely on these complex models and to put our trust in the simpler ones obtained by stratification.

The statistical models include only the predictors but no interactions among them, since they can be safely neglected, as we showed in PI. For each studied evolutionary feature, we included as covariates in the model only the physical input that can have an actual influence: for L_{BTO} and t_{H} the first four parameters of Table 1, and all the parameters for the quantities related to later evolutionary stages. The models were fitted to the data with a least-squares method using the software R 2.15.1 (R Development Core Team 2012).

For each Z value, for $\log L_{\text{BTO}}$ and t_{H} the regression models are

$$\log L_{\text{BTO}}, t_{\text{H}} = \beta_0 + \sum_{i=1}^4 \beta_i p_i \quad (1)$$

where β_0, \dots, β_4 were the regression coefficients to be estimated by the fit and p_1, \dots, p_4 the perturbation multipliers defined in Table 1.

In the cases of $\log L_{\text{tip}}$, $\log L_{\text{HB}}$, and M_{c}^{He} , the linear models for each Z value are

$$\log L_{\text{tip}}, \log L_{\text{HB}}, M_{\text{c}}^{\text{He}} = \beta_0 + \sum_{i=1}^7 \beta_i p_i \quad (2)$$

where we added the dependence on the triple- α reaction rate, the neutrino emission rate, and the conductive opacity k_c .

The cumulative effect of the physical input perturbation obtained from the statistical models for each evolutionary feature is listed in Table 2. There we report in the second column the reference value of the studied quantity obtained from the model with unperturbed physics, for each Z value, in the third column the cumulative statistical impact of the various physical inputs defined as $\sum_i \Delta p_i \times |\beta_i|$.

>From Table 2 some general trends are apparent. In the case of BTO log-luminosity, the total impact decreases with metallicity from $Z = 0.0001$ to 0.02 of about 40%. For central hydrogen exhaustion time, we note that the total impact grows with the metallicity with a rate slightly higher than the one of the increase in the reference time. In the case of RGB tip, we observe that the total impact on the luminosity is nearly constant at about 0.03 dex, whereas on the helium core mass it decreases from $0.0055 M_{\odot}$ at $Z = 0.0001$ to $0.0035 M_{\odot}$ at $Z = 0.02$. In the case of ZAHB luminosity, the effect of the chemical composition on the cumulative physical uncertainty is not monotonic. In this case the total impact shows an initially high value at $Z = 0.0001$, a sudden drop at $Z = 0.0005$, and a subsequent increase with the metallicity.

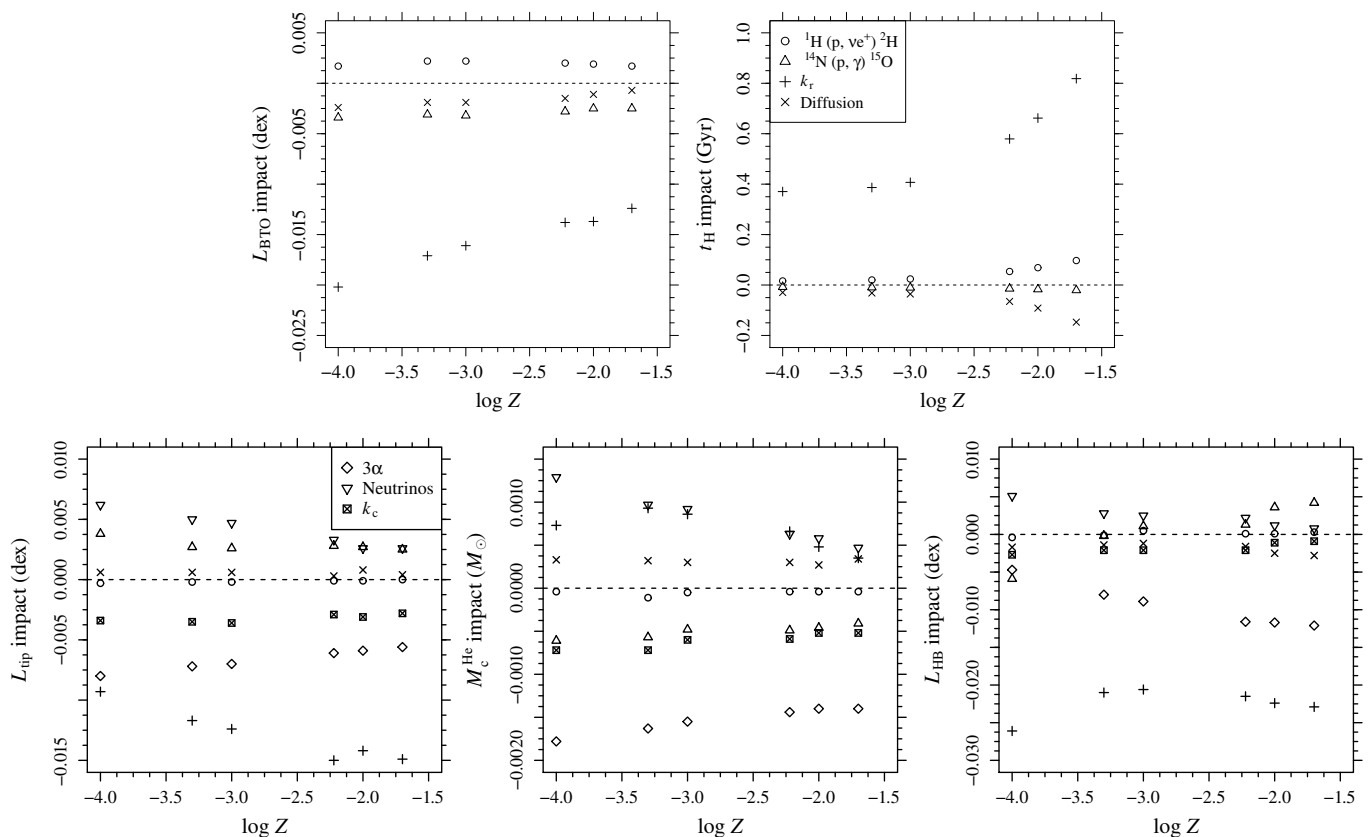


Fig. 1. Physical impacts – as in Tables A.3-A.7 – of the increment Δp_i of each multiplier p_i for the considered physical inputs at different $\log Z$ values.

In Fig. 1 we display the results of the fits for the different evolutionary quantities. This figure shows the physical impact of the increment Δp_i on each multiplier p_i in dependence on $\log Z$. The full results of the fits are reported in Tables A.3-A.7 (available online). These tables list, for different values of Z , the least squares estimations of the regression coefficients β_i , their standard error, the physical impact of the increment of Δp_i on each multiplier p_i , and the absolute value of the relative importance of these impacts with respect to the most important one.

In the case of $Z = 0.006$ the values of the estimated coefficients are different from the ones reported in PI, since the present estimates are obtained from a subsample of the original dataset. As expected, in almost all cases the present estimates and the ones of PI agree within their errors.

The figure and the tables show that the effect of perturbing the main physical input within their current uncertainty on the studied stellar evolutionary quantities changes in a rather complex way when varying the chemical composition. In particular, the relative importance of the various input physics in contributing to the global uncertainty changes with metallicity. As a consequence, one should be careful to extrapolate the results we obtained in PI for stellar models of $Z = 0.006$ to significantly different metallicities.

In the case of BTO luminosity, from Fig. 1 and from the last column of Table A.3, we note that the effect of the variation in radiative opacity is dominant for each value of Z , while the effect of the other physical inputs change mildly with metallicity. The second most important input is the one due to the $^{14}\text{N}(p,\gamma)^{15}\text{O}$ reaction rate at each Z . The impact of the perturbations scales almost linearly with $\log Z$.

For central hydrogen exhaustion time in Table A.4, it is apparent that the importance of radiative opacity is dominant for each Z and that the contribution of microscopic diffusion and of $^1\text{H}(p,ve)^2\text{H}$ reaction rate increase with metallicity. At $Z = 0.02$ they jointly account for about 30% of the impact of k_r . Figure 1 shows that the impact of the radiative opacity variation grows more than linearly with $\log Z$.

In the case of RGB tip luminosity, radiative opacity is the most important uncertainty source, but at lower Z its importance is close to the one of triple- α (87%) and neutrino cooling (67%); in contrast, for $Z = 0.02$ the cumulative impact of all the other sources of uncertainty is about 80% of the one of k_r . Figure 1 shows that the effect is due to the growth in the importance of the radiative opacities uncertainty with $\log Z$, with a concurrent decrease in the importance of the other sources of uncertainty.

For the helium core mass at RGB tip, the triple- α reaction rate is the most important uncertainty source. A distinctive feature is the decrease in the importance of neutrino cooling with increasing Z ; while it accounts for 72% of the impact of the triple- α at $Z = 0.0001$, this percentage decreases to 33% at $Z = 0.02$. We note also from Fig. 1 a non-monotonic trend with $\log Z$ for the radiative opacities effect.

For ZAHB luminosity, the radiative opacity is the main source of uncertainty at each metallicity. We observe from Fig. 1 an increase in the importance of triple- α moving toward high Z . A distinctive feature is the drop in the absolute value of the importance of radiative opacity from $Z = 0.0001$ to $Z = 0.0005$, followed by a mild increase with $\log Z$. The trend in the cumulative uncertainty is further complicated since the impact of $^{14}\text{N}(p,\gamma)^{15}\text{O}$, which is negative at $Z = 0.0001$, becomes positive at higher Z . Moreover, each physical input variation affects both

Table 2. Cumulative impact of the uncertainty on the physical inputs on the considered evolutionary features.

Z	Reference	Impact
$\log L_{\text{BTO}}$ (dex)		
0.0001	0.749	0.028
0.0005	0.648	0.024
0.0010	0.584	0.023
0.0060	0.354	0.020
0.0100	0.270	0.019
0.0200	0.151	0.017
t_{H} (Gyr)		
0.0001	7.21	0.42
0.0005	7.38	0.45
0.0010	7.74	0.48
0.0060	10.54	0.71
0.0100	12.32	0.84
0.0200	15.23	1.08
$\log L_{\text{tip}}$ (dex)		
0.0001	3.257	0.032
0.0005	3.315	0.031
0.0010	3.342	0.031
0.0060	3.406	0.030
0.0100	3.419	0.029
0.0200	3.431	0.029
M_{c}^{He} (M_{\odot})		
0.0001	0.5023	0.0055
0.0005	0.4936	0.0053
0.0010	0.4909	0.0048
0.0060	0.4836	0.0041
0.0100	0.4807	0.0037
0.0200	0.4750	0.0035
$\log L_{\text{HB}}$ (dex) at $\log T_{\text{eff}} = 3.83$		
0.0001	1.792	0.047
0.0005	1.701	0.036
0.0010	1.671	0.037
0.0060	1.565	0.041
0.0100	1.522	0.043
0.0200	1.465	0.044

Notes. First column: the metallicity of the stellar model; second column: the reference value for the model with unperturbed physical input; third column: the sum of the impacts of the analytical fit.

the He-core mass (and thus indirectly L_{HB}) and L_{HB} directly. These effects are the source of the non-monotonic trend on the cumulative uncertainty shown in Table 2. The precise understanding of the effect of each physical input is made even more difficult by the ZAHB luminosity being evaluated at fixed T_{eff} for all Z . This implies that at low Z the region is populated with higher masses with respect to the ones at high Z .

4. Physical uncertainty on stellar isochrones

The previous statistical analysis of the physical uncertainties affecting stellar tracks can be extended to isochrones. We focus here on isochrones with ages in the range 8-14 Gyr, which is suitable for galactic globular clusters. As in PI, we are interested in studying the variation near the turn-off region; so we performed calculations by varying only the physical input that can influence the evolution until this phase, i.e. p_1, \dots, p_4 . For each Z value, we selected stellar models from the full grid by varying p_1, \dots, p_4 (i.e. $3^4 = 81$ cases). Each metallicity grid

contains several stellar models with different masses, chosen to accurately reconstruct – in the desired age range – the BTO region. The computed stellar models are listed in Table A.8. A total of 5832 models and 3402 isochrones were calculated.

Following the technique outlined in PI, we pool together the results obtained from isochrones of different ages. For each Z we first remove the trend due to age by adapting an ANOVA model to the turn-off luminosity $\log L_{\text{BTO}}^{\text{iso}}$ and mass $M_{\text{BTO}}^{\text{iso}}$, with age as a categorical predictor. This method increases the power of the analysis due to the larger sample examined after pooling. The residuals of these models are then regressed against p_1, \dots, p_4 . Further details on the technique and discussion of the underlying hypotheses can be found in PI.

The results about the total uncertainty on $\log L_{\text{BTO}}^{\text{iso}}$ and $M_{\text{BTO}}^{\text{iso}}$, due to the simultaneous variation in all the considered input physics, are shown in Table 9. As in Sec. 3 the total uncertainty is obtained by adding the effect of each covariate. The total uncertainty on the reconstructed $\log L_{\text{BTO}}^{\text{iso}}$ and on the $M_{\text{BTO}}^{\text{iso}}$ shows a moderate increase with Z . In the case of $\log L_{\text{BTO}}^{\text{iso}}$ the difference between maximum and minimum uncertainty is of the order of 20%, whereas for $M_{\text{BTO}}^{\text{iso}}$ it is about 37%.

Table 9. Cumulative impact on the uncertainty on isochrone BTO luminosity (dex) and on the mass at isochrone BTO (M_{\odot}) for different metallicity values.

Z	Impact	
	$\log L_{\text{BTO}}^{\text{iso}}$ (dex)	$M_{\text{BTO}}^{\text{iso}}$ (M_{\odot})
0.0001	0.0118	0.0136
0.0005	0.0121	0.0141
0.0010	0.0122	0.0144
0.0060	0.0129	0.0164
0.0100	0.0138	0.0174
0.0200	0.0143	0.0186

Notes. The results are obtained by pooling together isochrones of ages in the range [8 - 14], see text for details.

Figure 2 and Tables 10-11 display the detailed results of the fits for $\log L_{\text{BTO}}^{\text{iso}}$ and $M_{\text{BTO}}^{\text{iso}}$. The figure displays the physical impact of the increment of Δp_i of each multiplier p_i in dependence on $\log Z$. The tables report, for different Z values, the least squares estimations of the regression coefficients β_i , their standard error, the physical impacts of the increment of Δp_i of each multiplier p_i , and the absolute value of the relative importance of these impact with respect to the most relevant one.

For $M_{\text{BTO}}^{\text{iso}}$ (Table 11) the relative contribution of the physical sources of uncertainty is almost the same for all the metallicity values; the only exception is the role of the p-p chain whose relative contribution to the cumulative uncertainty slightly increases with metallicity. The radiative opacity dominates over all the other physical input.

In the case of $\log L_{\text{BTO}}^{\text{iso}}$ (Table 10) the dependence on the chemical composition shows much more complex behaviour. At $Z = 0.0001$ the main contribution to the uncertainty comes from the microscopic diffusion velocities. At $Z = 0.001$ the effect of microscopic diffusion velocities, $^{14}\text{N}(p,\gamma)^{15}\text{O}$ reaction rate, and radiative opacity are similar; whereas at larger Z the effect of k_r becomes dominant. As shown in Table 9, these variation nearly compensate one another in the whole analysed range of metallicity, so that the cumulative uncertainty on $\log L_{\text{BTO}}^{\text{iso}}$ is nearly constant and ranges from 0.012 dex to 0.014 dex.

In Table 12 we present the results of the analysis on the uncertainty affecting the age inferred from BTO luminosity. We

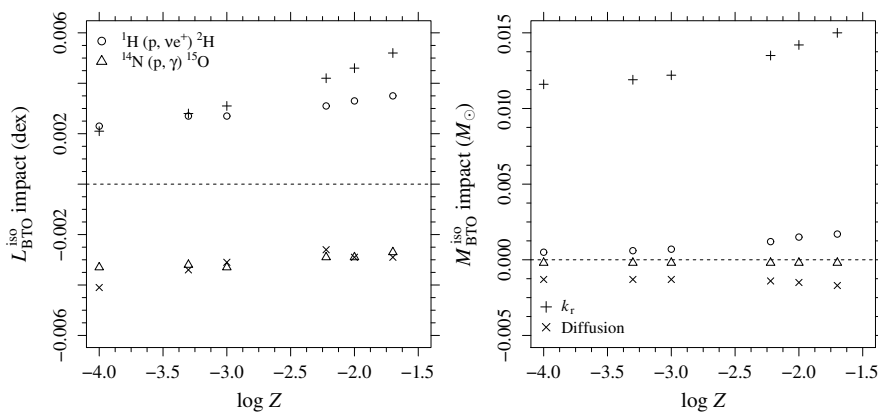


Fig. 2. Physical impacts on isochrone BTO luminosity and mass at isochrone BTO due to the increment Δp_i of each multiplier p_i for the considered physical inputs at different values of $\log Z$.

constructed – for each Z – linear models linking $\log L_{\text{BTO}}^{\text{iso}}$ and the logarithm of the age. We ignore the dependence on the physical inputs, confounding their effect with the residual standard error. The models are then used to perform a reverse inference on the value of the age, given $L_{\text{BTO}}^{\text{iso}}$. For each metallicity set, we fix the reference value of $\log L_{\text{BTO}}^{\text{iso}}$ to the one reached at 12 Gyr. More details about the technique are given in Appendix B of PI. The results collected in Table 12 show that the uncertainty in the inferred age increases by almost 30% from $Z = 0.0001$ to $Z = 0.02$, ranging from 325 Myr to 415 Myr.

5. Conclusions

In this paper we extended the work presented in Valle et al. (2013) that analyses the cumulative uncertainty due to physical inputs in stellar models of low-mass stars. The aim was to analyse the influence on the results of a variation in the assumed chemical composition. Thus we calculated stellar models for a wide range of metallicity from $Z = 0.0001$ to $Z = 0.02$.

For the stellar tracks, the cumulative physical uncertainty in the analysed quantities changes with the chemical composition. For turn-off luminosity the cumulative uncertainty decreases from 0.028 dex at $Z = 0.0001$ to 0.017 dex at $Z = 0.02$. The global uncertainty on the central hydrogen exhaustion time increases with Z from 0.42 Gyr to 1.08 Gyr, with a rate that is slightly higher than the increase in the reference time of hydrogen exhaustion at any given Z . In the case of the RGB tip, the cumulative uncertainty on the luminosity is almost constant at 0.03 dex, while on the helium core mass it decreases from $0.0055 M_{\odot}$ at $Z = 0.0001$ to $0.0035 M_{\odot}$ at $Z = 0.02$. The dependence on the metallicity of the error in the predicted ZAHB luminosity is not monotonic. The total uncertainty shows a value of 0.047 dex at $Z = 0.0001$, a sudden drop to a value of 0.036 dex at $Z = 0.0005$, and a following increase with Z up to a value of 0.044 dex at $Z = 0.02$.

We confirm the results presented in PI; i.e., for all the analysed stellar tracks features (except the He-core mass at the red giant branch tip), in the full adopted range of chemical compositions, the effects of the uncertainty on the radiative opacity tables is dominant. The uncertainty on the helium core mass at RGB tip is instead mainly due to the variation in the triple- α reaction rate. In conclusion, an increase in the precision of the radiative opacity tables is mandatory to further improve stellar evolution theoretical predictions.

For the stellar isochrones of 12 Gyr, the cumulative uncertainty on the predicted turn-off luminosity and mass show a moderate increase with Z . From $Z = 0.0001$ to 0.02, the global physical uncertainty increases of the order of 20% for $\log L_{\text{BTO}}^{\text{iso}}$ and 37% for $M_{\text{BTO}}^{\text{iso}}$. As a consequence, for ages in the range 8-14 Gyr, the uncertainty on the age inferred from the turn-off luminosity increases by about 30% from $Z = 0.0001$ to $Z = 0.02$, ranging from 325 Myr to 415 Myr.

Acknowledgements. We are grateful to our anonymous referee for pointing out a problem in the draft version and for several suggestions that helped in clarifying and improving the paper. This work has been supported by PRIN-INAF 2011 (*Tracing the formation and evolution of the Galactic Halo with VST*, P.I.M. Marconi).

References

- Carnell, R. 2012, lhs: Latin Hypercube Samples, r package version 0.10
- Chaboyer, B., Demarque, P., Kernan, P. J., Krauss, L. M., & Sarajedini, A. 1996, MNRAS, 283, 683
- Cyburtt, R. H., Fields, B. D., & Olive, K. A. 2004, Phys. Rev. D, 69, 123519
- Dell’Omodarme, M., Valle, G., Degl’Innocenti, S., & Prada Moroni, P. G. 2012, A&A, 540, A26
- Flynn, C. 2004, PASA, 21, 126
- Gennaro, M., Prada Moroni, P. G., & Degl’Innocenti, S. 2010, A&A, 518, A13+
- Irwin, A. W. 2004, <http://freeeos.sourceforge.net/documentation.html>
- Jimenez, R., Flynn, C., MacDonald, J., & Gibson, B. K. 2003, Science, 299, 1552
- Pagel, B. E. J. & Portinari, L. 1998, MNRAS, 298, 747
- Peimbert, M., Luridiana, V., & Peimbert, A. 2007a, ApJ, 666, 636
- Peimbert, M., Luridiana, V., Peimbert, A., & Carigi, L. 2007b, in Astronomical Society of the Pacific Conference Series, Vol. 374, From Stars to Galaxies: Building the Pieces to Build Up the Universe, ed. A. Vallenari, R. Tantaló, L. Portinari, & A. Moretti, 81–+
- R Development Core Team. 2012, R: A Language and Environment for Statistical Computing, R Foundation for Statistical Computing, Vienna, Austria, ISBN 3-900051-07-0
- Steigman, G. 2006, International Journal of Modern Physics E, 15, 1
- Stein, M. 1987, Technometrics, 29, 143
- Valle, G., Dell’Omodarme, M., Prada Moroni, P. G., & Degl’Innocenti, S. 2013, A&A, 549, A50
- Valle, G., Marconi, M., Degl’Innocenti, S., & Prada Moroni, P. G. 2009, A&A, 507, 1541

Appendix A: On the EOS influence

As discussed in PI, the uncertainty on the equation-of-state cannot be treated with the approach applied to the other physical input. To provide a rough estimate of the impact of the present uncertainty on EOS, we computed the reference tracks – i.e. the

Table 10. Effect of the various physical inputs on isochrones BTO luminosity (dex), for different Z values. The column legend is the same as in Table A.3.

	Estimate	Std. Error	Impact	Importance
$Z = 0.0001$				
β_0	-0.0591	0.0046		
β_1 (pp)	0.0775	0.0038	0.0023	0.573
β_2 (^{14}N)	-0.0332	0.0011	-0.0033	0.817
β_3 (k_r)	0.0418	0.0023	0.0021	0.515
β_4 (v_d)	-0.0271	0.0008	-0.0041	1.000
$Z = 0.0005$				
β_0	-0.0919	0.0041		
β_1 (pp)	0.0893	0.0034	0.0027	0.795
β_2 (^{14}N)	-0.0319	0.0010	-0.0032	0.945
β_3 (k_r)	0.0569	0.0020	0.0028	0.844
β_4 (v_d)	-0.0225	0.0007	-0.0034	1.000
$Z = 0.001$				
β_0	-0.0983	0.0038		
β_1 (pp)	0.0896	0.0031	0.0027	0.826
β_2 (^{14}N)	-0.0325	0.0009	-0.0033	1.000
β_3 (k_r)	0.0622	0.0018	0.0031	0.957
β_4 (v_d)	-0.0210	0.0006	-0.0031	0.968
$Z = 0.006$				
β_0	-0.1400	0.0027		
β_1 (pp)	0.1038	0.0022	0.0031	0.747
β_2 (^{14}N)	-0.0295	0.0007	-0.0029	0.707
β_3 (k_r)	0.0834	0.0013	0.0042	1.000
β_4 (v_d)	-0.0177	0.0004	-0.0026	0.635
$Z = 0.01$				
β_0	-0.1545	0.0031		
β_1 (pp)	0.1112	0.0026	0.0033	0.725
β_2 (^{14}N)	-0.0293	0.0008	-0.0029	0.637
β_3 (k_r)	0.0920	0.0015	0.0046	1.000
β_4 (v_d)	-0.0195	0.0005	-0.0029	0.635
$Z = 0.02$				
β_0	-0.1738	0.0031		
β_1 (pp)	0.1164	0.0025	0.0035	0.673
β_2 (^{14}N)	-0.0273	0.0008	-0.0027	0.526
β_3 (k_r)	0.1038	0.0015	0.0052	1.000
β_4 (v_d)	-0.0191	0.0005	-0.0029	0.553

ones with unperturbed physics – with two different and widely adopted choices for equation-of-state: OPAL EOS and FreeEOS (Irwin 2004).

Table A.1 reports – for each evolutionary feature and for each Z – the impact of the EOS change. A comparison of these values with the one of the “Impact” column in Table 2 shows that the EOS change accounts for about 10% to 20% of the total impact of all the other physical input. The only exception is the helium core mass: in this case the impact of the EOS variation accounts for 20% to 40% of the total impact of the other physical input.

Table 11. Effect of the various physical inputs on the masses at isochrones BTO (M_\odot), for different Z values. The column legend is the same as in Table A.3.

	Estimate	Std. Error	Impact	Importance
$Z = 0.0001$				
β_0	-0.2388	0.0019		
β_1 (pp)	0.0165	0.0016	0.0005	0.042
β_2 (^{14}N)	-0.0019	0.0005	-0.0002	0.016
β_3 (k_r)	0.2328	0.0009	0.0116	1.000
β_4 (v_d)	-0.0086	0.0003	-0.0013	0.110
$Z = 0.0005$				
β_0	-0.2480	0.0015		
β_1 (pp)	0.0207	0.0012	0.0006	0.052
β_2 (^{14}N)	-0.0023	0.0004	-0.0002	0.019
β_3 (k_r)	0.2382	0.0007	0.0119	1.000
β_4 (v_d)	-0.0086	0.0002	-0.0013	0.108
$Z = 0.001$				
β_0	-0.2558	0.0015		
β_1 (pp)	0.0238	0.0012	0.0007	0.059
β_2 (^{14}N)	-0.0025	0.0004	-0.0002	0.020
β_3 (k_r)	0.2432	0.0007	0.0122	1.000
β_4 (v_d)	-0.0087	0.0002	-0.0013	0.107
$Z = 0.006$				
β_0	-0.2998	0.0021		
β_1 (pp)	0.0413	0.0017	0.0012	0.092
β_2 (^{14}N)	-0.0024	0.0005	-0.0002	0.018
β_3 (k_r)	0.2702	0.0010	0.0135	1.000
β_4 (v_d)	-0.0093	0.0003	-0.0014	0.103
$Z = 0.01$				
β_0	-0.3200	0.0015		
β_1 (pp)	0.0493	0.0012	0.0015	0.104
β_2 (^{14}N)	-0.0023	0.0004	-0.0002	0.016
β_3 (k_r)	0.2833	0.0007	0.0142	1.000
β_4 (v_d)	-0.0103	0.0002	-0.0015	0.109
$Z = 0.02$				
β_0	-0.3438	0.0018		
β_1 (pp)	0.0576	0.0014	0.0017	0.115
β_2 (^{14}N)	-0.0016	0.0004	-0.0002	0.011
β_3 (k_r)	0.2994	0.0009	0.0150	1.000
β_4 (v_d)	-0.0115	0.0003	-0.0017	0.115

Table 12. Uncertainty on the age inferred from the BTO luminosity. The uncertainty is evaluated around 12 Gyr.

Z	Uncertainty (Gyr)
0.0001	0.325
0.0005	0.345
0.0010	0.355
0.0060	0.345
0.0100	0.365
0.0200	0.415

Table A.1. Impact of equation of state change from OPAL to FreeEOS for the examined evolutionary features

Z	$\log L_{\text{BTO}}$ (dex)	t_{H} (Gyr)	$\log L_{\text{tip}}$ (dex)	M_{c}^{He} (M_{\odot})	$\log L_{\text{HB}}$ (dex)
0.0001	0.0017 (6%)	0.053 (13%)	0.0022 (7%)	-0.00095 (17%)	-0.0039 (8%)
0.0005	0.0025 (10%)	0.049 (11%)	0.0005 (2%)	-0.00117 (22%)	-0.0037 (10%)
0.0010	0.0031 (13%)	0.057 (12%)	-0.0006 (2%)	-0.00132 (28%)	-0.0046 (12%)
0.0060	0.0028 (14%)	0.096 (13%)	-0.0020 (7%)	-0.00149 (36%)	-0.0070 (17%)
0.0100	0.0023 (12%)	0.110 (13%)	-0.0027 (9%)	-0.00142 (38%)	-0.0030 (7%)
0.0200	0.0031 (18%)	0.192 (18%)	-0.0027 (9%)	-0.00115 (33%)	-0.0013 (3%)

Notes. In parenthesis: percentage influence of EOS change with respect to the values in the column “Impact” of Table 2.

Table A.3. Estimated coefficients for the linear model in Eq. 1 of BTO luminosity (dex), for different Z values.

	Estimate (dex)	Std. Error (dex)	Impact (dex)	Importance
$Z = 0.0001$				
β_0	1.1455	0.0026		
β_1 (pp)	0.0581	0.0020	0.0017	0.086
β_2 (^{14}N)	-0.0338	0.0006	-0.0034	0.167
β_3 (k_r)	-0.4050	0.0012	-0.0202	1.000
β_4 (v_d)	-0.0160	0.0004	-0.0024	0.119
$Z = 0.0005$				
β_0	0.9593	0.0027		
β_1 (pp)	0.0730	0.0021	0.0022	0.128
β_2 (^{14}N)	-0.0312	0.0006	-0.0031	0.183
β_3 (k_r)	-0.3411	0.0012	-0.0171	1.000
β_4 (v_d)	-0.0124	0.0004	-0.0019	0.109
$Z = 0.001$				
β_0	0.8775	0.0026		
β_1 (pp)	0.0735	0.0020	0.0022	0.137
β_2 (^{14}N)	-0.0315	0.0006	-0.0032	0.195
β_3 (k_r)	-0.3229	0.0012	-0.0161	1.000
β_4 (v_d)	-0.0124	0.0004	-0.0019	0.115
$Z = 0.006$				
β_0	0.6031	0.0028		
β_1 (pp)	0.0650	0.0021	0.0020	0.141
β_2 (^{14}N)	-0.0278	0.0006	-0.0028	0.202
β_3 (k_r)	-0.2760	0.0012	-0.0138	1.000
β_4 (v_d)	-0.0098	0.0004	-0.0015	0.106
$Z = 0.01$				
β_0	0.5144	0.0030		
β_1 (pp)	0.0620	0.0023	0.0019	0.136
β_2 (^{14}N)	-0.0250	0.0007	-0.0025	0.183
β_3 (k_r)	-0.2737	0.0014	-0.0137	1.000
β_4 (v_d)	-0.0074	0.0005	-0.0011	0.081
$Z = 0.02$				
β_0	0.3715	0.0025		
β_1 (pp)	0.0571	0.0019	0.0017	0.138
β_2 (^{14}N)	-0.0248	0.0006	-0.0025	0.200
β_3 (k_r)	-0.2484	0.0011	-0.0124	1.000
β_4 (v_d)	-0.0044	0.0004	-0.0007	0.053

Notes. In the first two columns: least-squares estimates of the regression coefficients and their errors; third column: physical impact of the variation Δp_i of the various inputs; last column: relative importance of the impact with respect to the most important one.

Table A.4. Estimated coefficients for the linear model in Eq. 1 of the central hydrogen exhaustion time (Gyr), for different Z values. The column legend is the same as in Table A.3.

	Estimate (Gyr)	Std. Error (Gyr)	Impact (Gyr)	Importance
$Z = 0.0001$				
β_0	-0.4596	0.0115		
β_1 (pp)	0.5368	0.0089	0.016	0.043
β_2 (^{14}N)	-0.0776	0.0027	-0.008	0.021
β_3 (k_r)	7.4100	0.0052	0.370	1.000
β_4 (v_d)	-0.1982	0.0017	-0.030	0.080
$Z = 0.0005$				
β_0	-0.7055	0.0105		
β_1 (pp)	0.6674	0.0081	0.020	0.052
β_2 (^{14}N)	-0.0965	0.0024	-0.010	0.025
β_3 (k_r)	7.7301	0.0047	0.387	1.000
β_4 (v_d)	-0.2115	0.0016	-0.032	0.082
$Z = 0.001$				
β_0	-0.8548	0.0130		
β_1 (pp)	0.8001	0.0101	0.024	0.059
β_2 (^{14}N)	-0.1047	0.0030	-0.011	0.026
β_3 (k_r)	8.1423	0.0059	0.407	1.000
β_4 (v_d)	-0.2379	0.0020	-0.036	0.088
$Z = 0.006$				
β_0	-2.2543	0.0306		
β_1 (pp)	1.7872	0.0237	0.054	0.092
β_2 (^{14}N)	-0.1437	0.0071	-0.014	0.025
β_3 (k_r)	11.5876	0.0139	0.579	1.000
β_4 (v_d)	-0.4341	0.0046	-0.065	0.112
$Z = 0.01$				
β_0	-2.4268	0.0421		
β_1 (pp)	2.2898	0.0325	0.069	0.104
β_2 (^{14}N)	-0.1721	0.0097	-0.017	0.026
β_3 (k_r)	13.2384	0.0191	0.662	1.000
β_4 (v_d)	-0.6116	0.0064	-0.092	0.139
$Z = 0.02$				
β_0	-3.1791	0.0600		
β_1 (pp)	3.2350	0.0464	0.097	0.119
β_2 (^{14}N)	-0.2074	0.0139	-0.021	0.025
β_3 (k_r)	16.3678	0.0272	0.818	1.000
β_4 (v_d)	-0.9817	0.0091	-0.147	0.180

Table A.5. Estimated coefficients for the linear model in Eq. 2 of RGB tip luminosity (dex), for different Z values. The column legend is the same as in Table A.3.

	Estimate (dex)	Std. Error (dex)	Impact (dex)	Importance
$Z = 0.0001$				
β_0	3.3628	0.0120		
β_1 (pp)	-0.0086	0.0077	-0.0003	0.028
β_2 (^{14}N)	0.0377	0.0023	0.0038	0.405
β_3 (k_r)	-0.1858	0.0046	-0.0093	1.000
β_4 (v_d)	0.0041	0.0015	0.0006	0.066
β_5 (3α)	-0.0402	0.0011	-0.0080	0.866
β_6 (ν)	0.1552	0.0057	0.0062	0.668
β_7 (k_c)	-0.0676	0.0047	-0.0034	0.364
$Z = 0.0005$				
β_0	3.5049	0.0109		
β_1 (pp)	-0.0062	0.0070	-0.0002	0.016
β_2 (^{14}N)	0.0271	0.0021	0.0027	0.231
β_3 (k_r)	-0.2349	0.0041	-0.0117	1.000
β_4 (v_d)	0.0037	0.0014	0.0006	0.047
β_5 (3α)	-0.0362	0.0010	-0.0072	0.616
β_6 (ν)	0.1258	0.0051	0.0050	0.428
β_7 (k_c)	-0.0693	0.0042	-0.0035	0.295
$Z = 0.001$				
β_0	3.5569	0.0101		
β_1 (pp)	-0.0069	0.0065	-0.0002	0.017
β_2 (^{14}N)	0.0256	0.0019	0.0026	0.206
β_3 (k_r)	-0.2478	0.0039	-0.0124	1.000
β_4 (v_d)	0.0039	0.0013	0.0006	0.048
β_5 (3α)	-0.0351	0.0010	-0.0070	0.566
β_6 (ν)	0.1171	0.0048	0.0047	0.378
β_7 (k_c)	-0.0719	0.0039	-0.0036	0.290
$Z = 0.006$				
β_0	3.6840	0.0024		
β_1 (pp)	-0.0020	0.0015	-0.0001	0.004
β_2 (^{14}N)	0.0277	0.0005	0.0028	0.185
β_3 (k_r)	-0.2997	0.0009	-0.0150	1.000
β_4 (v_d)	0.0021	0.0003	0.0003	0.021
β_5 (3α)	-0.0303	0.0002	-0.0061	0.404
β_6 (ν)	0.0816	0.0011	0.0033	0.218
β_7 (k_c)	-0.0574	0.0009	-0.0029	0.192
$Z = 0.01$				
β_0	3.7028	0.0132		
β_1 (pp)	-0.0048	0.0085	-0.0001	0.010
β_2 (^{14}N)	0.0267	0.0025	0.0027	0.188
β_3 (k_r)	-0.2845	0.0050	-0.0142	1.000
β_4 (v_d)	0.0054	0.0017	0.0008	0.057
β_5 (3α)	-0.0296	0.0013	-0.0059	0.416
β_6 (ν)	0.0641	0.0062	0.0026	0.180
β_7 (k_c)	-0.0616	0.0051	-0.0031	0.216
$Z = 0.02$				
β_0	3.7215	0.0116		
β_1 (pp)	0.0000	0.0075	0.0000	0.000
β_2 (^{14}N)	0.0249	0.0022	0.0025	0.167
β_3 (k_r)	-0.2988	0.0044	-0.0149	1.000
β_4 (v_d)	0.0030	0.0015	0.0004	0.030
β_5 (3α)	-0.0280	0.0011	-0.0056	0.374
β_6 (ν)	0.0642	0.0055	0.0026	0.172
β_7 (k_c)	-0.0553	0.0045	-0.0028	0.185

Table A.6. Estimated coefficients for the linear model in Eq. 2 of helium core mass M_c^{He} (M_\odot) for different Z values. The column legend is the same as in Table A.3.

	Estimate (M_\odot)	Std. Error (M_\odot)	Impact (M_\odot)	Importance
$Z = 0.0001$				
β_0	0.4839	0.0042		
β_1 (pp)	-0.0013	0.0027	-0.0000	0.023
β_2 (^{14}N)	-0.0061	0.0008	-0.0006	0.344
β_3 (k_r)	0.0147	0.0016	0.0007	0.411
β_4 (v_d)	0.0022	0.0005	0.0003	0.185
β_5 (3α)	-0.0089	0.0004	-0.0018	1.000
β_6 (ν)	0.0323	0.0020	0.0013	0.724
β_7 (k_c)	-0.0143	0.0016	-0.0007	0.402
$Z = 0.0005$				
β_0	0.4806	0.0021		
β_1 (pp)	-0.0037	0.0013	-0.0001	0.069
β_2 (^{14}N)	-0.0057	0.0004	-0.0006	0.353
β_3 (k_r)	0.0186	0.0008	0.0009	0.573
β_4 (v_d)	0.0021	0.0003	0.0003	0.196
β_5 (3α)	-0.0081	0.0002	-0.0016	1.000
β_6 (ν)	0.0242	0.0010	0.0010	0.596
β_7 (k_c)	-0.0144	0.0008	-0.0007	0.442
$Z = 0.001$				
β_0	0.4749	0.0017		
β_1 (pp)	-0.0017	0.0011	-0.0001	0.033
β_2 (^{14}N)	-0.0048	0.0003	-0.0005	0.312
β_3 (k_r)	0.0172	0.0006	0.0009	0.555
β_4 (v_d)	0.0020	0.0002	0.0003	0.194
β_5 (3α)	-0.0077	0.0002	-0.0015	1.000
β_6 (ν)	0.0230	0.0008	0.0009	0.596
β_7 (k_c)	-0.0120	0.0007	-0.0006	0.388
$Z = 0.006$				
β_0	0.4779	0.0004		
β_1 (pp)	-0.0013	0.0003	-0.0000	0.027
β_2 (^{14}N)	-0.0049	0.0001	-0.0005	0.338
β_3 (k_r)	0.0131	0.0001	0.0007	0.456
β_4 (v_d)	0.0020	0.0001	0.0003	0.209
β_5 (3α)	-0.0072	0.0000	-0.0014	1.000
β_6 (ν)	0.0158	0.0002	0.0006	0.440
β_7 (k_c)	-0.0119	0.0002	-0.0006	0.412
$Z = 0.01$				
β_0	0.4782	0.0015		
β_1 (pp)	-0.0012	0.0010	-0.0000	0.026
β_2 (^{14}N)	-0.0046	0.0003	-0.0005	0.331
β_3 (k_r)	0.0095	0.0006	0.0005	0.340
β_4 (v_d)	0.0018	0.0002	0.0003	0.195
β_5 (3α)	-0.0070	0.0001	-0.0014	1.000
β_6 (ν)	0.0145	0.0007	0.0006	0.413
β_7 (k_c)	-0.0104	0.0006	-0.0005	0.372
$Z = 0.02$				
β_0	0.4769	0.0015		
β_1 (pp)	-0.0015	0.0010	-0.0000	0.031
β_2 (^{14}N)	-0.0041	0.0003	-0.0004	0.292
β_3 (k_r)	0.0070	0.0006	0.0003	0.249
β_4 (v_d)	0.0023	0.0002	0.0003	0.244
β_5 (3α)	-0.0070	0.0001	-0.0014	1.000
β_6 (ν)	0.0117	0.0007	0.0005	0.334
β_7 (k_c)	-0.0103	0.0006	-0.0005	0.369

Table A.7. Estimated coefficients for the linear model in Eq. 2 of the ZAHB luminosity $\log L_{\text{HB}}$ at $\log T_{\text{eff}} = 3.83$ (dex) for different Z values. The column legend is the same as in Table A.3.

	Estimate (dex)	Std. Error (dex)	Impact (dex)	Importance
$Z = 0.0001$				
β_0	2.3509	0.0168		
β_1 (pp)	-0.0150	0.0108	-0.0004	0.017
β_2 (^{14}N)	-0.0594	0.0032	-0.0059	0.227
β_3 (k_r)	-0.5224	0.0064	-0.0261	1.000
β_4 (v_d)	-0.0113	0.0021	-0.0017	0.065
β_5 (3α)	-0.0237	0.0016	-0.0047	0.182
β_6 (ν)	0.1267	0.0079	0.0051	0.194
β_7 (k_c)	-0.0539	0.0065	-0.0027	0.103
$Z = 0.0005$				
β_0	2.1457	0.0091		
β_1 (pp)	-0.0019	0.0058	-0.0001	0.003
β_2 (^{14}N)	-0.0015	0.0017	-0.0002	0.007
β_3 (k_r)	-0.4209	0.0035	-0.0210	1.000
β_4 (v_d)	-0.0093	0.0012	-0.0014	0.066
β_5 (3α)	-0.0399	0.0009	-0.0080	0.380
β_6 (ν)	0.0712	0.0043	0.0028	0.135
β_7 (k_c)	-0.0420	0.0035	-0.0021	0.100
$Z = 0.001$				
β_0	2.0878	0.0121		
β_1 (pp)	0.0163	0.0078	0.0005	0.024
β_2 (^{14}N)	0.0106	0.0023	0.0011	0.052
β_3 (k_r)	-0.4126	0.0046	-0.0206	1.000
β_4 (v_d)	-0.0078	0.0015	-0.0012	0.057
β_5 (3α)	-0.0446	0.0012	-0.0089	0.432
β_6 (ν)	0.0623	0.0057	0.0025	0.121
β_7 (k_c)	-0.0415	0.0047	-0.0021	0.101
$Z = 0.006$				
β_0	2.0339	0.0045		
β_1 (pp)	0.0040	0.0029	0.0001	0.006
β_2 (^{14}N)	0.0133	0.0009	0.0013	0.062
β_3 (k_r)	-0.4304	0.0017	-0.0215	1.000
β_4 (v_d)	-0.0109	0.0006	-0.0016	0.076
β_5 (3α)	-0.0579	0.0004	-0.0116	0.538
β_6 (ν)	0.0556	0.0021	0.0022	0.103
β_7 (k_c)	-0.0427	0.0017	-0.0021	0.099
$Z = 0.01$				
β_0	1.9961	0.0067		
β_1 (pp)	0.0045	0.0043	0.0001	0.006
β_2 (^{14}N)	0.0362	0.0013	0.0036	0.161
β_3 (k_r)	-0.4489	0.0025	-0.0224	1.000
β_4 (v_d)	-0.0168	0.0009	-0.0025	0.112
β_5 (3α)	-0.0583	0.0006	-0.0117	0.520
β_6 (ν)	0.0309	0.0032	0.0012	0.055
β_7 (k_c)	-0.0215	0.0026	-0.0011	0.048
$Z = 0.02$				
β_0	1.9478	0.0056		
β_1 (pp)	0.0084	0.0036	0.0003	0.011
β_2 (^{14}N)	0.0425	0.0011	0.0042	0.185
β_3 (k_r)	-0.4588	0.0021	-0.0229	1.000
β_4 (v_d)	-0.0189	0.0007	-0.0028	0.124
β_5 (3α)	-0.0603	0.0005	-0.0121	0.526
β_6 (ν)	0.0211	0.0027	0.0008	0.037
β_7 (k_c)	-0.0172	0.0022	-0.0009	0.037

Table A.8. Stellar models computed for isochrones construction at different Z values.

Z	Stellar models (M_{\odot})
0.0001	0.50, 0.60, 0.70, 0.72, 0.75, 0.77, 0.80, 0.82, 0.85, 0.87, 0.90, 0.95
0.0005	0.50, 0.60, 0.70, 0.72, 0.75, 0.77, 0.80, 0.82, 0.85, 0.87, 0.90, 0.95
0.0010	0.50, 0.60, 0.70, 0.75, 0.77, 0.80, 0.82, 0.85, 0.87, 0.90, 0.92, 0.95
0.0060	0.50, 0.60, 0.70, 0.80, 0.85, 0.87, 0.90, 0.92, 0.95, 1.00, 1.05, 1.10
0.0100	0.70, 0.80, 0.85, 0.87, 0.90, 0.92, 0.95, 0.97, 1.00, 1.02, 1.05, 1.10
0.0200	0.70, 0.80, 0.85, 0.87, 0.90, 0.92, 0.95, 0.97, 1.00, 1.02, 1.05, 1.10